

Multi-Mode 3D Ultrasonic Phased Array Imaging Method Using Piezoelectric and Laser Ultrasonic System (PLUS)

Yoshikazu Ohara^{1†}, T. J. Ulrich², Marcel C. Remillieux², Kosuke Tsunoda¹, Takumi Yamada¹, Toshihiro Tsuji¹, and Tsuyoshi Mihara¹ (¹Tohoku Univ.; ²Los Alamos National Laboratory)

1. Introduction

Nondestructive evaluation of defects is vital to ensure the safety and reliability of structures and mechanical components. Ultrasonic phased array (PA) is one of the widely used imaging methods in industrial fields. Most PAs use a 1D array transducer, producing 2D images. On the other hand, actual defects can have complex 3D geometries. Achieving more sophisticated management of structures and mechanical components would require the development of a 3D imaging method. The PA with a 2D matrix array transducer is a promising approach. To this end, a 2D matrix array transducer should have more than 32×32 (i.e., 1024) elements to obtain a high spatial resolution in 3D imaging, given that 1D array transducers typically have 32-128 elements. However, such an array transducer is unacceptable for industrial fields in terms of cost. To open up a new avenue to 3D PA imaging, we proposed a piezoelectric and laser ultrasonic system (PLUS).¹⁻³ The PLUS combines a piezoelectric transmitter and a mechanical scan of a laser Doppler vibrometer (LDV) to create a 2D matrix array with ultra-multiple elements.

In this study, we propose multi-mode PLUS to enhance its imaging capability and attain more robustness. Thus far, PLUS uses a single mode (longitudinal or shear scattered waves). However, the scattering at defects can accompany the mode conversion, which has been deftly utilized for a nonlinear ultrasonic phased array.⁴ After describing the concept of multi-mode PLUS, we show the imaging algorithm with a formulation of delay laws. We also examined the validity of the imaging algorithm using a simulated received waveform dataset for a scatterer.

2. Principle of Multi-Mode PLUS

The PLUS combines a monolithic piezoelectric transmitter and a 2D matrix array receiver based on the 2D scanning of an LDV, as illustrated in **Fig. 1**. An ultrasonic wave is emitted into a sample at an incident angle by a piezoelectric transducer mounted on a wedge. An incident wave is scattered at defects. Note that the scattering phenomena can accompany

the mode conversion. The scattered waves are then received at a point on the top surface by an LDV. The same process is repeated while moving the receiving point over a scan area. Here, the LDV receiving points correspond to the elements of a piezoelectric array transducer. Hence, the ultra-multiple elements of a 2D matrix array can be readily realized by increasing the number of receiving points, e.g., to the order of thousands, which is much higher than the maximum number of elements for a piezoelectric array transducer. A large-amplitude ultrasonic incidence by a piezoelectric transmitter can compensate for the intrinsically low sensitivity of the LDV.

Multi-mode PLUS uses both longitudinal and mode-converted shear waves, respectively. To utilize both modes, we formulate the propagation time corresponding to the delay laws for the longitudinal (LL) and mode-converted shear (LS) scattered waves, respectively, for a longitudinal-wave incidence. The propagation time from the transmitter \mathbf{r}_T through a focal point \mathbf{r} to an element $\mathbf{r}_{nx,ny}$ of the array transducer are respectively expressed for LL and LS waves as follows;

$$t_{nx,ny}(\mathbf{r}) = \frac{|\mathbf{r}_T - \mathbf{r}_I|}{V_W} + \frac{|\mathbf{r} - \mathbf{r}_I|}{V_L} + \frac{|\mathbf{r}_{nx,ny} - \mathbf{r}|}{V_L}, \quad (1)$$

$$t_{nx,ny}(\mathbf{r}) = \frac{|\mathbf{r}_T - \mathbf{r}_I|}{V_W} + \frac{|\mathbf{r} - \mathbf{r}_I|}{V_L} + \frac{|\mathbf{r}_{nx,ny} - \mathbf{r}|}{V_S}, \quad (2)$$

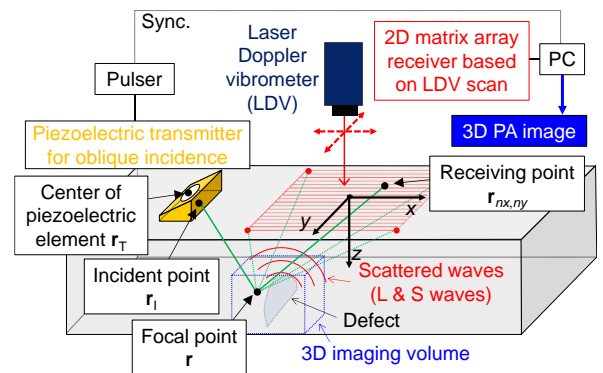


Fig. 1 Schematics of a 3D PA imaging system, PLUS.

where V_L and V_S are the longitudinal- and shear-wave speeds in a sample, respectively, V_W is the longitudinal-wave speed in the wedge, n_x and n_y are the indices of the receiving point in the x - and y -directions, respectively, and \mathbf{r}_I is the incident point on the interface between the transmitter and the sample. By repeating this delay-and-sum (DAS) processing based on Eqs. (1) and (2), respectively, over an imaging volume, 3D images for LL and LS modes can be created without any additional experiment.

3. Fundamental Investigation of Multi-Mode PLUS for a Scatterer by Simulation

For the theoretical demonstration of multi-mode PLUS, 3D numerical simulation, e.g., by finite element method (FEM), would be useful. However, such a simulation is not easy because of the computation cost for 3D. Hence, under the following assumption,³⁾ we simulated the received waves at each acquisition point based on the propagation time given by Eqs.(1) and (2), respectively. We first assume that the incident wave is $s(t)$ and a scatterer generates a spherically scattered wave. A received wave at an acquisition point is expressed by

$$u_{n_x, n_y}(t) = s\left(t - t_{n_x, n_y}(\mathbf{r}_S)\right). \quad (3)$$

We assumed incident and scattered waves propagate in an isotropic sample at $V_L=6260$ and $V_T=3080$ m/s as transverse waves. For simplicity, no attenuation was considered. The incident wave was simulated using a Hanning-windowed burst wave (5 MHz, 3 cycles). The number of receiving points was 4047 (i.e., 71×57) and the center of the receiving area was $x=y=z=0$. The pitch between the adjacent receiving points was fixed to 0.5 mm in the x - and y -directions. The single scatterer (\mathbf{r}_S) was set at $x=-23$ mm, $y=0$ mm, and $z=29.5$ mm. Under the assumption of the above condition, we prepared the complete dataset of received waves using Eq. (3). Subsequently, we applied the DAS processing based on Eqs. (1) and (2) over the imaging volume of $26 \times 26 \times 26$ mm³ with a pitch of 0.5 mm.

Figures 2(a) and 2(b) shows the 3D imaging results obtained with the imaging algorithms for L-L and L-S modes, where the responses of scattering intensity above a threshold were displayed. **Figure 3** shows the B-scan images extracted from the 3D imaging results of Fig. 2. For both modes, the scatterer was visualized at the correct position. This validates the imaging algorithm for multi-mode PLUS. The spatial resolution in the imaging results for the LS mode was higher than those for the LL mode. This is because of the difference in the wavelength between the longitudinal and shear waves.

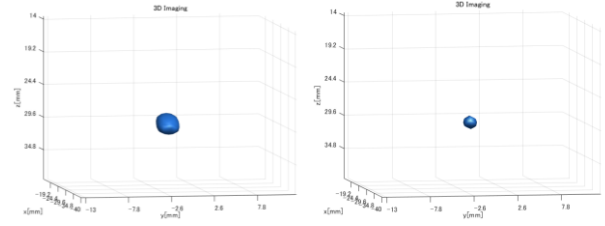


Fig. 2 3D imaging results of simulated received waveforms for a point scatterer based on longitudinal and mode-converted shear waves .

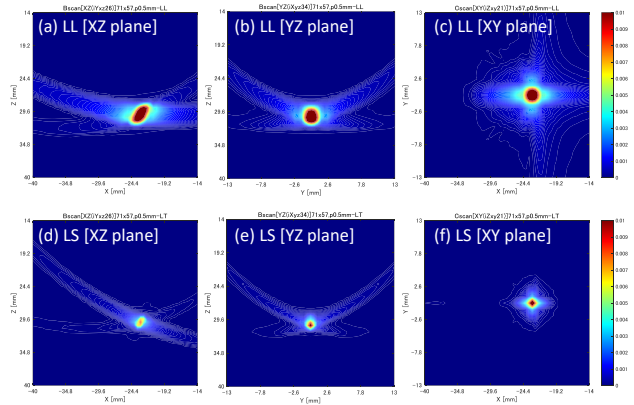


Fig. 3 B-scan image extracted from the 3D imaging results of Fig. 2; (a)-(c) B-scan images in XZ -, YZ -, XY -planes, respectively, for LL mode. (d)-(f) B-scan images in XZ -, YZ -, XY -planes, respectively, for LS mode.

4. Conclusions

We proposed multi-mode PLUS to enhance its imaging capability and attain more robustness. After describing the concept of multi-mode PLUS with the formulation of the delay laws, we examined its fundamental performance based on the simulated received waves from a scatterer. Although the simulation assumed a spherical scattering for simplicity, the scattering behaviors at actual defects can change depending on the modes and can be more complicated.^{3,4)} We will conduct an experimental investigation to demonstrate the usefulness of multi-mode PLUS at actual defects.

Acknowledgments

This work was partially supported by JSPS KAKENHI (19K20910, 21H04592, and 22K18745) and JST FOREST Program (JPMJFR2023).

References

1. Y. Ohara, et al.: APL **117** (2020) 111902.
2. Y. Ohara, et al.: JJAP **61** (2022) SG1043.
3. Y. Ohara, et al.: Sci. Rep. **12** (2022) 8291.
4. Y. Ohara, et al: JJAP **58** (2019) SGGB06.